ELSEVIER

Check for updates

The working principle of hybrid perovskite gamma-ray photon counter

Fangze Liu [1], Michael Yoho [2], Hsinhan Tsai [1], Kasun Fernando [1], Jeremy Tisdale [1], Shreetu Shrestha [1], Jon K. Baldwin [1], Aditya D. Mohite [3], Sergei Tretiak [1,4], Duc T. Vo [2], Wanyi Nie [1,*]

[1] Center for Integrated Nanotechnology, Material Physics and Application Division, Los Alamos National Laboratory, Los Alamos, NM 87545, United States
[2] Safeguards Science and Technology, Nuclear Engineering and Nonproliferation Division, Los Alamos National Laboratory, Los Alamos, NM 87545, United States
[3] Chemical and Biomolecular Engineering, Rice University, Houston, TX 77005, United States
[4] Physics and Chemistry of Materials, Theory Division, Los Alamos National Laboratory, Los Alamos, NM 87545, United States

Gamma-ray spectroscopy that quantifies the gamma-ray energies is a critical technology widely needed in astrophysics, nuclear material detection and medical treatment. The key is to precisely count gamma-ray photons using sensitive detectors. In this paper, we investigate the operational principles of chlorine-doped methylammonium lead tribromide ($MAPbBr_{3-x}Cl_x$) perovskite single crystal detectors that can efficiently count gamma-ray photon events with electrical pulses. Specifically, we find the main dark current originates from the thermally activated electron injection from the impurities, and using high work function contacts can block out the dark noise thus allows for efficient pulse collection at higher electrical fields ~500 V/cm. As a result, we observe strong electrical pulses when exposing the detector under radioactive sources emitting gamma-ray photons at various energies. Our results also reveal the fundamental issues that prevent the reliable observation of photo-electric peak. This work suggest pathway towards energy resolved gamma-ray spectroscopy using perovskite crystal detectors.

Introduction

Gamma-ray spectroscopy is a critical technology that underpins a wide range of applications including medical diagnosis [1,2], astronomy [3,4], advanced photon experiments [5,6] and nuclear material activity monitoring [7,8]. A sensitive detector capable of detecting gamma-ray photons with high count rate and sharp energy resolutions, is essentially the key to successfully implement it into those applications. In recent years, solid-state detectors using monocrystalline semiconductors have shown a great promise in resolving gamma-ray spectra with superior sensitivities by directly converting the gamma-ray photon into electrical signal [9]. The detection principle is based on the physical processes of gamma-ray photon interaction with heavy atoms in the semiconducting materials [10]. The schematic diagrams and expected signals are described in Fig. 1. Specifically, when a gamma-ray photon enters the semiconductor, it either completely deposits its energy on the atoms or is inelastically scattered from the atoms, depositing only a fraction of its energy. The former is called photo-electrical effect and the latter refers to Compton scattering. Both processes will ionize a number of electron-hole pairs and directly collecting all the carriers from the device yields an electrical pulse signal that corresponds to a single gamma-ray photon ionization event. In addition, low amplitude pulses can be observed caused by 180° scattering events by the atoms (back scattering). The energy is thus resolved

* Corresponding author.
E-mail address: Nie, W. (wanyi@lanl.gov)

1369-7021/Published by Elsevier Ltd. https://doi.org/10.1016/j.mattod.2020.02.022

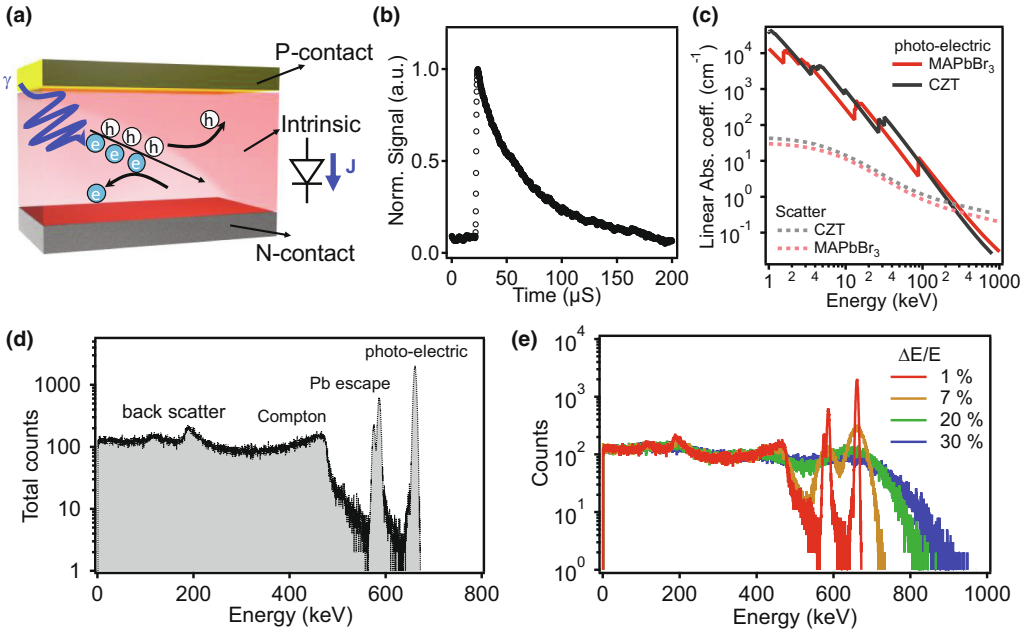

FIGURE 1

The working principle of solid-state gamma-ray detector. (a) Schematic illustration of gamma-ray detector structure and charge ionization process. (b) A typical pulse from CZT detector under ^{137}Cs radiation source. (c) Calculated linear absorption cross-section coefficient of photo-electric effect and scatter process as a function of gamma-ray photon energy of CZT and $MAPbBr_3$ crystals. (c) and (e) Simulated gamma-ray detector spectra for 5 mm by 5 mm by 1 mm $MAPbBr_3$ single crystal device by Monte Carlo simulation for: (d) detector with 1% energy resolution and (e) detectors simulated with several different energy resolutions.

by the statistics of the pulse amplitude, where full energy deposition events generate a sharp photo-electric peak directly corresponding to the energy of the gamma ray, and the Compton process is represented as a continuous band at lower energy which does not contribute to the energy resolution. Thus, based on this working principle, a typical spectrum should consist of photo-electric peak, metal escape peak, Compton edge and back scattering features [11].

To successfully construct the energy resolved spectra, it is crucial to obtain a reliable electrical pulse induced by each gamma-ray semiconductor interaction event with appreciable signal to noise ratio. Therefore, a successful demonstration of a solid-state gamma-ray detector requires optimization of several important device characteristics. Firstly, the dark current of the detector needs to be minimized so that the electronics can resolve pulse signals at all amplitude for spectrum construction. Secondly, to collect all the ionized charges caused by a single incident gamma-ray photon, a large bias is required during the detector operation. Thirdly, an ideal semiconductor for gamma-ray detector must comprise heavy elements to efficiently interact with gamma-ray photons while maintaining excellent transport properties (i.e. mobility-lifetime (μ-τ) product) in order to maximize the photo-electric peak that contributes to the spectra. To fulfill the above requirements, a *p-i-n* device configuration is often chosen where a highly resistive intrinsic semiconductor is sandwiched between *p* and *n* contacts (Fig. 1a). The detector is also operated under large reverse bias (>1000 V/cm) to ensure efficient pulse collections, while the *p-i-n* device design blocks out the dark current induced noise.

The benchmark industry-standard solid-state detectors employ Germanium (Ge) or Cadmium Zinc Telluride (CZT) single crystals. The former provides an excellent energy resolution at 77 K and the latter is more promising at room temperature. Recently, lead halide perovskite semiconductors were recognized as promising materials for X-ray [5,12–22] and gamma-ray detection [15,23–26] at room temperature with low-cost fabrication process [27,28]. They have many attractive properties as solid-state gamma-rays detectors, such as the presence of heavy elements (Pb, Cs, Br and I), excellent transport properties with large mobility-lifetime (μ-τ) products [15,23,24,26]. Calculation shows that the linear absorption cross-section coefficient for methylammonium lead tribromide ($MAPbBr_3$) via photo-electric effect is very high across a large energy range (Fig. 1c, red line), and is comparable to the widely used classical CZT semiconductors (black line) from 1 keV to 1 MeV. In addition, the absorption through scattering process in $MAPbBr_3$ is relatively low in the energy range of 1–600 keV compared to the photo-electric process, suggesting a good probability of ionizing charges via photo-electric effect in the perovskite crystals. We run Monte Carlo simulations (see supplementary methods for details of the simulation) for $5 \times 5 \times 1$ mm^3 $MAPbBr_3$ single crystal with ^{137}Cs radiation source to generate the gamma-ray spectra. The expected spectra are plotted in Fig. 1d and e with different energy resolutions. When the energy is well resolved at 1% resolution by the $MAPbBr_3$ perovskite detector, several features should be observed. The photo-electric peak at 662 keV and lead escape peak around 587 keV are both significant in the perovskite crystal as shown in Fig. 1d. The Compton edge and back scatter peaks at lower energies are also expected. When the resolution is low (i.e. > 10 %) as shown in Fig. 1e, the photo-electric peak is merged with the Pb escape peak and forms a broadened feature which is merely separated from the Compton edge. Based on the

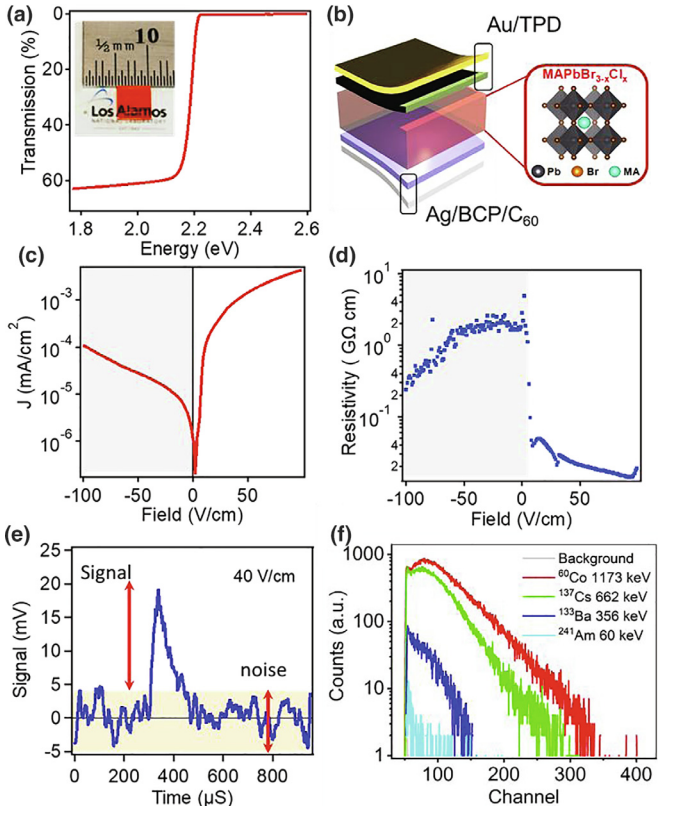

FIGURE 2

Perovskite single crystal characterizations and initial results on gamma-ray detector fabricated in *p-i-n* device structure. (a) The photo of a typical crystal with 5 × 5 × 2 mm in dimension and its optical transmission spectrum. (b) *p-i-n* device structure using $MAPbBr_{3-x}Cl_x$ used for this part of the study. (c) Dark current density–electric field characteristics for a typical *p-i-n* junction device and (d) the extracted dark resistivity as a function of applied electrical field. (e) A typical one Gamma-ray pulse obtained from $MAPbBr_{3-x}Cl_x$ detector operated under −8 V. (f) Gamma-ray spectra when expose the device under various radioactive sources collected by a multi-channel analyzer (MCA) when the detector was operated at −8 V at room temperature.

discussion above, the high absorption cross-section and expected sharp photo-electric peak along with the low Compton shoulder motivate the further study on the lead halide perovskites-based gamma ray detector.

Several initial studies demonstrated promising perovskite detectors operating at room temperatures. For example, Yakunin et al. reported the first energy resolved gamma-ray spectrum from ^{241}Am at 59.6 keV with 35% energy resolution using solution grown $FAPbI_3$ single crystal [26]. Wei et al. used dopant compensated $MAPbBr_{3-x}Cl_x$ crystals to increase the bulk resistivity and achieved below 10% energy resolution at 662 keV from ^{137}Cs radiation at a field of 18 V/cm [24]. He et al. achieved energy resolution of 12% at 59.6 keV from ^{241}Am and 6.8% at 122 keV from ^{57}Co with $MAPbI_3$ single crystals at 2 °C using asymmetric Schottky-type electrodes [15]. In addition to organic–inorganic lead halide perovskites, all-inorganic perovskite $CsPbBr_3$ single crystals were also proven to be high performing for gamma-ray detection with energy resolution approaching the industrial standard CZT detectors when operating under 7×10^3 V/cm [23]. While those demonstrations are highly promising, especially the latter three are intriguing, their working conditions are very different despite all claimed high energy resolution <10%. For example, the $MAPbI_3$ detector and $MAPbBr_{3-x}Cl_x$ detector operate under 400 V/cm and 18 V/cm respectively. All three type of detectors, $MAPbBr_{3-x}Cl_x$, $CsPbBr_3$ and $MAPbI_3$, can work under room temperature while a slight cooling to 2 °C can significantly improve the resolution of $MAPbI_3$. The reported energy detection ranges are also very different. While the $CsPbBr_3$ detectors can detect the widest range of energy from 32.3 keV to 662 keV, $MAPbI_3$ detectors only work for low energy gamma-ray (59.5 keV and 122 keV) and $MAPbBr_{3-x}Cl_x$ detectors only work for high energy gamma-ray (662 keV). Therefore, the exact response of hybrid perovskite solid-state detectors towards gamma-ray photons are under explored. Specifically, the fundamental detector response parameter, such as the electrical pulses generated from the gamma-ray photon as discussed above, are not well understood. Therefore, an in-depth study on the gamma-ray photon induced pulses and detector operational principle is critically needed in order to push perovskite detector towards the use in high resolution gamma-ray spectroscopy.

In this work, we investigate the operational principle of the gamma-ray photon counting device made with $MAPbBr_{3-x}Cl_x$ single crystals. Specifically, we observed strong electrical pulses with appreciable signal to noise ratio from the detector that are associated to the incident gamma-ray photon events. This is achieved by blocking electron injected from defect that contributes to the dark current noise with high work function contacts. In-depth device characteristics reveal that the hole transport occurs through band conduction regime in the $MAPbBr_{3-x}Cl_x$ system which suppresses the thermally injected dark current at large electrical field and contributes to the efficient pulse counting. Meanwhile, an unusually long rise time of the electrical pulse at room temperature was observed from the $MAPbBr_{3-x}Cl_x$ device, it shows weak dependence on the bias voltage but drastically decreases when temperature is lowered. We attribute it to the slow ion motion in the bromide crystal under fields. Finally, we obtained gamma-ray energy spectra by counting pulses near room temperature using a customized setup. Based on the pulse statistics, the expected spectrum structure was successfully constructed that resembles the Compton scattering edge and counts from photo-electric peaks. Our study focuses on the gamma-ray photon counting mechanism using hybrid perovskite crystals; it reveals the critical role of reducing dark current and pulse rise time for efficient pulse collection that lays foundation for spectrum constructions which are missing from previous studies on $MAPbBr_{3-x}Cl_x$ crystals.

Results

Detector made with p-i-n junction configuration

We first grow chlorine-doped $MAPbBr_{3-x}Cl_x$ (Fig. 2a) single crystals following the well-established "inverse temperature growth" approach [27,28]. The obtained crystals are in the 1–5 mm length range at thickness values of 1–3 cm with cubic phase crystal structure. Fig. 2a shows the photograph and the optical transmission of a typical crystal. The transmission of the crystal below the band gap, i.e., wavelength above 570 nm, was found to be greater than 60%, suggesting a good quality of the bulk crystal that is free

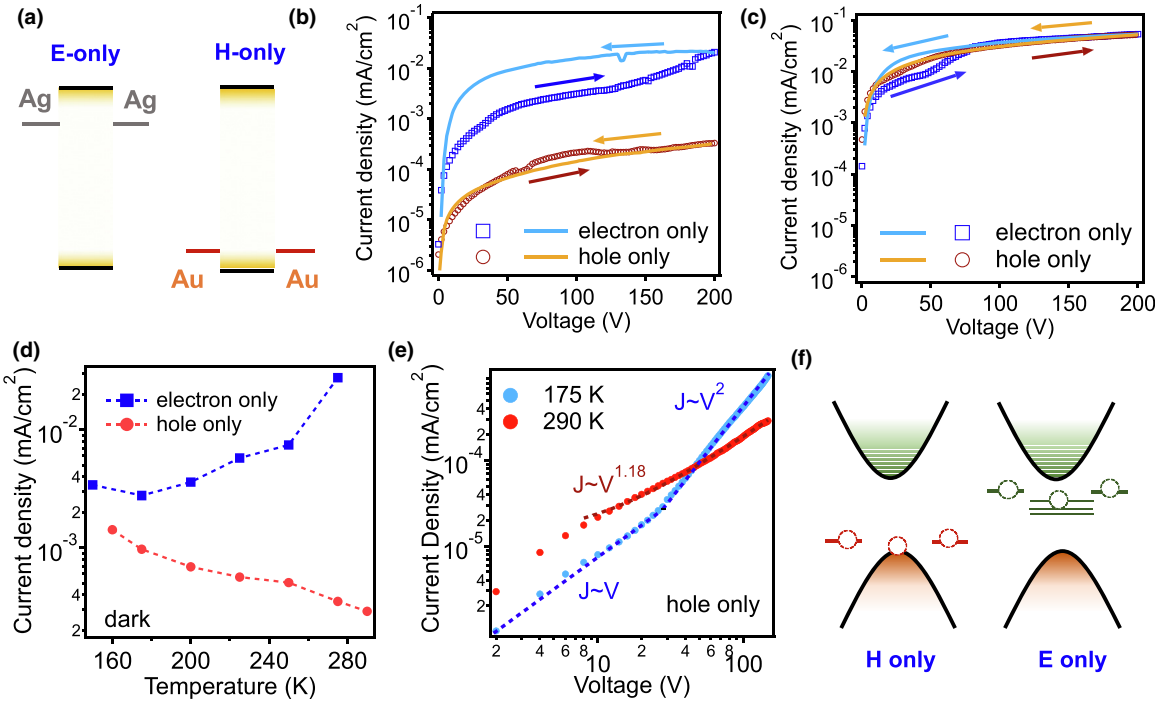

FIGURE 3

Dark and photo current density–voltage (*J-V*) characterizations for electron only and hole only devices. (a) Band diagram schematic for electron-only (E-only) and hole only (H-only) devices. The *J-V* hysteresis curves for E-only and H-only devices in (b) dark and (c) under white light. Arrows point to the voltage sweeping direction. (d) The current density values at 180 V as a function of temperature for E-only (blue) and H-only (red) devices. (e) Log-log plot of the H-only device in dark at 290 K and 175 K, dotted lines are linear fittings. (f) Cartoon illustration of the charge transport mechanism in the E-only and H-only devices.

of optical scattering from bulk impurity or surface roughness (see Fig. S1 in SI for the photoluminescence spectrum).

We further incorporated the grown crystals into detectors in a *p-i-n* junction configuration, where the p-contact is Au/N,N′-Bis (3-methylphenyl)-N,N′-diphenylbenzidine (TPD) deposited on one side, and the n-contact is formed with fullerene (C_{60})/Bathocuproine (BCP)/Ag on the other side (Fig. 2b). A typical dark current density-electric field (*J-E*) characteristic is plotted in Fig. 2c. The estimated the dark resistivity is 1×10^9 Ω m at low reverse bias. It has been shown that the incorporation of chlorine (6%) in the crystal ($MAPbBr_{3-x}Cl_x$) can reduce the dopant density [24]. Our $MAPbBr_{3-x}Cl_x$ crystals here also have comparable high resistivity with both *p-i-n* or *p-i-p* device configurations. However, the dark resistivity at reverse bias does not remain flat and drops drastically to 2×10^8 Ω cm when the field is higher than −50 V/cm. When placing the device under the various radiation sources, the device responses are shown in Fig. 2e and f. Fig. 2e is a typical ^{137}Cs gamma-ray induced pulse at a bias of −40 V/cm (See Fig. S2 in SI for pulses from several devices). The pulse height is 20 mV with ~4 mV background noise. In Fig. 2f, the spectra are constructed using multichannel analyzer (MCA, see SI Fig. S3 for instrument diagram). The gray curve is the dark background noise without sources. The spectra under various sources (^{60}Co, ^{133}Ba, ^{137}Cs and ^{241}Am) are clearly above the dark background, suggesting that the detector actively responds to the gamma-ray radiation. The spectrum does shift to a higher channel number as the gamma-ray energy increases because the pulse amplitude increases accordingly. However, we do not observe any spectral shape for this device that should include the Compton edge and the photoelectric peaks like in the simulated spectrum in Fig. 1d and e. Moreover, the device can only work for several minutes before the background noise significantly increases. In most cases, the device can recover to low noise state without applying any voltage for a few minutes. The comparison of background noise is plotted in Fig. S4. Furthermore, the highest electrical field that could be applied to any *p-i-n* device, is only 50 V/cm before the dark noise overwhelms gamma-ray signal at room temperature. This is because of the rapid drop in the dark resistivity at the high bias that introduces large current noise despite of the low average dark current at low electric fields. The lack of a high electric field during the detector operation significantly limits the detector performance since this is essential to enhance charge collection efficiency and to ensure high spectral resolution.

The mechanism for the observed dark current

In an intrinsic semiconductor when the background doping density is low, the observations of a large dark current are often attributed to the dark recombination through trap states [29,30]. Fabricating *p-i-n* device helps to reduce the low dark current with interface blocking layers. However, it is still too high in this case to obtain an appreciable pulse-to-noise ratio for operation as a single gamma-ray photon counter. To understand the origin of the large dark noise in our *p-i-n* device, we fabricated symmetric devices with *p*-type (Au) and *n*-type (Ag) contacts (schematics of the relative band diagrams are shown in Fig. 3a) on both sides to examine the electron only and hole only

currents separately in dark, light and at various temperatures. The results are summarized in Fig. 3.

Dark and photo current of electron (E) and hole (H) only devices are shown in Fig. 3b and c, where the arrows indicate the voltage sweeping direction. It is clear that the E-only device current density is two orders of magnitude higher than that of the H-only device in the dark. Furthermore, a severe *J-V* hysteresis in the E-only device is observed, whereas the forward and reverse *J-V* curves overlay much better in the H-only device. Upon illuminating the devices with white light, the photo-currents for both devices arrive at comparable values (Fig. 3c). To gain deeper insight to the device working mechanism, we further investigated the temperature dependence of the *J-V* curves in the dark. The extracted current density values at 180 V are plotted in Fig. 3d against the temperature. It is interesting that the E-only current density shows a high value at room temperature and drastically reduces by 10 times at lower temperature. This suggests the electron current is thermally activated at room temperature, which usually originates from the trap assisted recombination. On the contrary, the H-only current density systematically increases when temperature decreases. In Fig. 3e, we fit the *J-V* characteristics for the H-only device with power law $J \sim V^{\alpha}$ equation. At room temperature, the *J-V* curve follows almost linear dependence for the whole region. When temperature is reduced to 175 K, two distinct slopes are observed: (1) low bias regime (0–30 V), where $\alpha = 1$, and the current increases linearly with voltage following the Ohm's law; (2) high bias regime (30–200 V), where $\alpha = 2$, and the H-only device is in the SCL region. The SCL current can be calculated by the Mott-Gurney law [31]

$$j = \frac{9}{8}\varepsilon_s \varepsilon_0 \mu \frac{V^2}{d^3}$$

where ε_s and ε_0 are the material dielectric constant and the vacuum permittivity, respectively, μ is the charge mobility, V is the voltage and d refers to the thickness. Within the tested temperature range of 150 K to 290 K, the carrier scattering is dominated by phonon interaction, and thus μ increases as temperature decreases. Previously, a high α value ($\alpha > 2$) has been found in perovskite crystals as a characterization for trap states as traps are quickly filled and contribute to the majority of current [27]. We notice that the trap filling region with a high α value ($\alpha > 2$) is not observed for the H-only device in this voltage range. This suggests the H-only device behaves as expected without the influence of charge trapping at high injection rate.

Based on the experimental analysis above, we conclude that in the $MAPbBr_{3-x}Cl_x$ system, the electron and hole transports have distinctly different nature as depicted in Fig. 3f. The electron current follows a thermally activated process and reduces with temperature. This suggests the electrons are conducting through the hopping mechanism via the local trap states below the gap. In contrast, the hole transport is closer to classical band conduction [32], and the current here is representative of the hole mobility. It exhibits negative temperature dependence due to reduced charge scattering by phonons at low temperature. The photoconductivity values of both type of carriers are similar suggesting that the traps are passivated by illumination in the E-only device, and the transport mechanism follows band transport (See temperature dependence of photocurrent data in Fig. S5). We note that the Ag contact is known to react with $MAPbI_3$ and forms AgI at the interface. However, this is a slow process taking several days to detect the existence of AgI under air exposure. In our case, to protect the device from ambient air, all metal depositions and sample characterizations were performed either in argon filled glove box or high vacuum ($<10^{-5}$ torr). The detector measurements were done immediately after Ag deposition and finished within one day. To check the device stability, we also compared J-V curves of the E-only device in five days, shown in Fig. S6, and found the change in current density was tiny. Thus, we conclude that the E-only devices were not affected by the reaction between Ag and perovskite.

Gamma-ray induced pulses using hole only devices

After understanding the device operational mechanism and the physical origin of the dark current, we next characterize the gamma-ray detector responses using the *p-i-p* device structure that gives lower dark current and robust dark resistivity under high electric field (>100 V/cm).

Fig. 4a plots the resistivity of H- and E-only devices. The resistivity for H-only device stays constantly above 10^9 Ω/cm, while

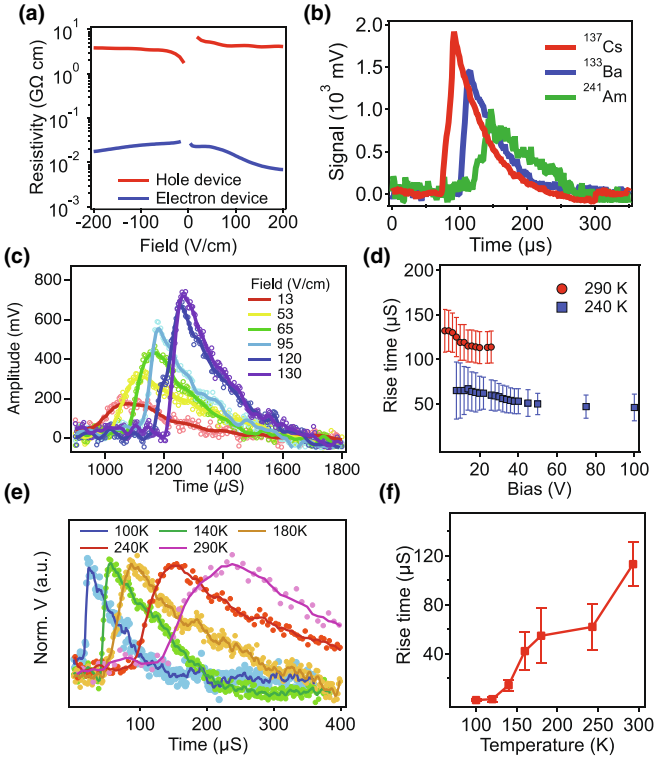

FIGURE 4

Gamma-ray detector demonstration with pulses and study of the pulse rise time. (a) Extracted dark resistivity of the H-only device (red) and E-only device (blue). (b) Electrical pulses under various radioactive sources when the detector was operated under 400 V/cm at 260 K. Note that the pulse height is not necessarily proportional to the gamma-ray energy. The difference in pulse height only represents a statistical trend. (c) Typical gamma-ray induced electrical pulses from the H-only device when exposed under ^{137}Cs source at room temperature (290 K) with various electrical fields. (d) Averaged rise time of the H-only detector as a function of applied bias at 290 K and 240 K. (e) Typical pulses at various temperature and 20 V bias under ^{137}Cs source. The pulses are shifted horizontally to show the rising edge. (f) Averaged rise time as a function of temperature.

that for E-only device is about two orders of magnitude lower and rapidly drops at high electric field. We then compare the dark current density between perovskite H-only and CZT devices at room temperature with a similar crystal size, as plotted in Fig. S8 in Supplementary Information. The dark current of our best perovskite device is still about 4 times higher than the reference CZT device and is comparable with reported lowest value achieved for hybrid perovskite crystals [24]. Indeed, no gamma-ray generated pulse can be extracted from the E-only device due to the high background current noise. On the contrary, many pulses under different gamma-ray sources are consistently collected in the H-only device as shown in Fig. 4b when the detector was operated at 400 V/cm at slightly reduced temperature (260 K). The pulse signals are well above the noise, the signal-to-noise ratios are 19 (^{131}Cs) and 10 (^{124}Am) respectively, 2–4 times higher than the *p-i-n* device in Fig. 2. The pulse amplitude increases consistently when the gamma-ray energy gets higher across different radioactive sources as expected. Fig. 4c displays typical pulses from our solid-state perovskite detector when exposed to ^{137}Cs source and driving at various bias voltages. The measured pulses show greatly enhanced amplitude to noise ratio from 4 to 10 when bias increases from 13 V/cm to 130 V/cm at room temperature. This suggests higher electrical field applied on the detector is crucial for efficient pulse counting. Note that up to 150 V/cm can now be applied to most of the *p-i-p* perovskite devices at room temperature for few hours without producing considerable noise that completely overwhelms the signal from gamma-ray photons. This is attributed to the large dark resistivity which remains flat with increasing electrical field (Fig. 4a).

Interestingly, we notice the long rise time is still present in this device configuration. To quantitatively analyze the effect of temperature and bias voltage, we plot the rise time at two temperatures (290 K and 240 K) versus the bias voltage in Fig. 4c. The averaged rise time is calculated by averaging 100 pulses under each voltage. Notably the average rise time drops at room temperature only moderately from (132 ± 24) μs to (113 ± 18) μs when the bias increases from 2 to 26 V. Once the temperature reduces to 240 K, on the other hand, the rise time is much smaller (65 ± 32) μs at 8 V and further drops to (46 ± 15) μs at 100 V. These results clearly suggest that decreasing temperature has more pronounced effect compared to the increasing voltage in reducing the pulse rise time.

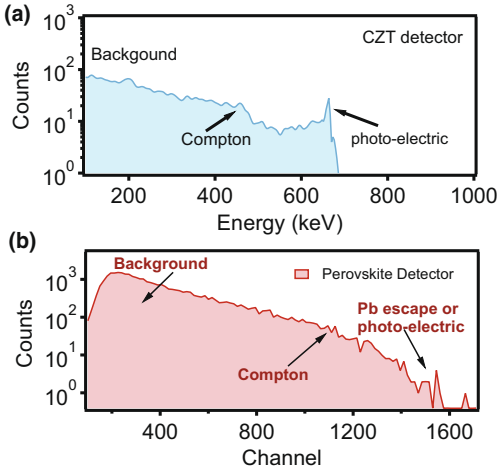

FIGURE 5

Gamma-ray detector spectra constructed with the pulses collected under ^{137}Cs sources with 1-h accumulation at room temperature. Spectrum in (a) is for the standard CZT detector and (b) is our perovskite single carrier detector operated under 225 V/cm. The *X*-axis in (b) are the channel numbers from pulse histogram.

To better understand the rise time, we further performed the temperature dependent measurements in a liquid-nitrogen-cooled cryostat under medium vacuum (10^{-6} torr). Representative pulses under the same field (100 V/cm) and ^{137}Cs radiation are normalized and plotted in Fig. 4e. The averaged rise time is extracted from the pulses and plotted against temperature in Fig. 4f. From Fig. 4e, the detector outputs much cleaner and sharper signals at low temperature and the pulses rise rapidly within 10 μs at 100 K, which is the fastest rise time than the other reported detectors based for organic–inorganic perovskite ($MAPbI_3$ and $MAPbBr_{3-x}Cl_x$) [24,26]. In Fig. 4f, we analyzed 100 pulses for each temperature and plotted the average rise time as a function of temperature. The histogram of the rise time is shown in Fig. S9. We found the rise time of the pulses decreases almost exponentially, indicating the limiting factor for the slow rise time of the detector, is thermally activated processes. In perovskite materials, the ionic motions are considered to be significant under applied fields. The charge transport is sometimes coupled to the structural change, such as lattice dynamics or ion migration [33–35]. We performed temperature dependent impedance spectroscopy of the H-only device, shown in Fig. S12. Under low frequency (<1000 Hz) and high temperature (>200 K), the capacitance is high and dominated by the slow ion migration [36,37]. Once the temperature is slightly reduced, the capacitance drops quickly and become flat below 200 K as the ion migration is strongly suppressed. Comparing with the rise time graph in Fig. 4f, the average rise time continues to decrease below 200 K and reaches minimum around 120 K. The continuous drop in rise time below 200 K may come from reduced ion migration below the detection limit of the impedance spectroscopy or other effects such as defects [38] and phase transitions [39]. Further studies of gamma-ray generated charge transport of perovskite crystals are required to completely understand and improve the performance of perovskite gamma-ray detector.

Motivated by the clean pulses obtained at higher applied voltages, with slightly reduced temperatures, we count and accumulate the pulses for longer times and construct the energy spectra based on the pulse statistics. However, we notice many of the commercial multichannel analyzers (MCA) are designed to process pulses faster than 12 μs from commercial detectors. To obtain the true spectrum for the perovskite detectors featuring longer rise times, we collected the pulses using an Oscilloscope (Tektronix DPO4104) or a customized Pixie-Net multichannel digital pulse processor, and constructed the spectra with customized post pulse processing (see Fig. S3 for setup diagram). We first validate the instrument setup using a CZT detector working at 500 V under a ^{137}Cs source and Fig. 5a is the spectrum accumulated for 600 seconds. From the detector spectra, we were able to resolve the ^{137}Cs gamma-ray photo-electric peak with an energy resolution of about 2 % and a clear Compton edge. The

large background in the CZT spectrum could be from the inefficient pulse collection from our home-built system and noises introduced during the long accumulation process. Fig. 5b shows a ^{137}Cs spectrum acquired from an H-only perovskite device at 240 K operated under 45 V bias voltage with 1000 seconds accumulation using the same experiment setup as the CZT detector. The Compton edge and backscatter features are not as clear as the CZT spectrum at low channel numbers (low energy). This may be attributed to the low energy resolution as seen from Fig. 1e that once the energy resolution is above 20%, all spectral features become indistinguishable. Apart from that, we also found some counts at higher energy that may correspond to the photo-electric peak or lead escape peak.

Discussion

By investigating the charge transport and the detector operation mechanisms, we arrive at a conclusion that ability to increase pulse height and reduce pulse rise time are the key foundation for constructing reliable energy resolved spectrum. Operating at single photon counting mode casts stringent requirement on maximizing the signal to noise ratio, which mandates an efficient charge collection throughout the bulk crystal and across the interfaces at high electric fields. In the $MAPbBr_{3-x}Cl_x$ system, we find that a large dark resistivity that should also be robust under high electric fields, is critically needed in order to count the pulses efficiently induced by gamma-ray photons. When the dark recombination dominates charge transport (electron injection through the trap states) and introduces high dark current, the noise overwhelms the pulse signal and makes the pulse collection challenging. In our demonstration, making H-only device by blocking all the electron recombination with high work function contacts, significantly reduces the dark noise and leads to a clear discrimination of gamma-ray induced pulses. It also helps to stabilize the detector under high electric field that allows for long time pulse accumulations. As a result, we were able to observe strong electrical pulses corresponding to the gamma-ray photon and semiconductor interaction events from the detector with an appreciable signal-to-noise ratio over 10, and for various radioactive sources.

On the other hand, an unusually long rise time from the $MAPbBr_{3-x}Cl_x$ detector was observed, reminiscent of slow pulses observed in other published work [15,26]. This remains a problem when using most of the commercial MCAs for pulse analysis, since these are designed for fast pulses. To construct the spectrum, the home-built setup that can capture those slow pulses, was employed. By counting the pulses, we were able to reconstruct a reliable spectrum that includes Compton edge and counts at photo-electric peaks. We also notice that the number of high amplitude pulses in $MAPbBr_{3-x}$ Cl_x are very low which based on our discussion in Fig. 1, mainly contributes to the photo-electrical peak. Even when the detector is cooled at 77 K (Fig. S10 and S11 in SI) where all the dark noise was suppressed, the photo-electric peak is still missing whereas the Compton edge and back scattering peaks can be resolved. This can be attributed to the poor charge separation efficiency in the bromide system with strong exciton binding energies [40,41]. To further improve the detector performance towards room temperature operation with high resolution photo-electric peaks, clean and robust perovskite crystals lacking ion migration under high electric fields, are needed.

Materials and methods

Materials

N,N′-Bis(3-methylphenyl)-N,N′-diphenylbenzidine (TPD), fullerene (C60), Bathocuproine(BCP), lead bromide (99% purity) and methylammonium bromide (≥99% purity), methylammonium chloride, N,N-Dimethylformamide (DMF) were purchase from Sigma-Aldrich and used as received.

Crystal growth and characterization

We employed inverse temperature growth technique for the $MAPbBr_{3-x}Cl_x$ crystals. Specifically, we dissolve lead bromide (99% purity) and methylammonium bromide as well as methylammonium chloride powders with a molar ratio of 1:1.2:0.5 dissolved in DMF solution. The temperature was ramped slowly from room temperature to 80 °C at a rate of 4 °C per hour that yielded a large crystal with high transparency. Absorption spectrum was measured by a Jasco V-730 UV–Visible Spectrophotometer in reflection mode.

Device fabrication

Metal contact materials (Au and Ag) were deposited by e-beam evaporation through a shadowed mask. The organic interfacial layers such as fullerene and TPD were deposited by thermal evaporation with the same shadow mask.

Device testing

Transport measurements were performed in a Janis probe station equipped with Keithley 2400 source meter and Keithley 6517B high resistance electrometer. The chamber was pumped down to 10^{-5} torr and the temperature was controlled by a LakeShore model 330 temperature controller. The gamma-ray detectors were mounted by attaching silver wires with silver paste on the device to external wires connecting to BNC cables. The assembled detectors were encapsulated in glass vials under argon condition, the pre-attached wires come through the cap and were sealed by epoxy to prevent degradation caused by the ambient air. Low temperature measurements were done by mounting the detectors in a Janis liquid nitrogen cryostat and pumped under intermediate vacuum of 10^{-6} torr. The detectors were tested by connecting them to a ORTEC 142PC charge sensitive pre-amplifier from which the high bias was applied. The output signal was amplified and filtered through a SR530 amplifier and then connected to a ORTEC DSPEC Pro, Tektronix DPO4104 oscilloscope or PixieNet multi-channel digital pulse processor for pulse collection and processing (Fig. S3 in Supplementary information). Radioactive source used were 0.21 μCi ^{241}AM, 99 μCi ^{133}Ba, 230 μCi ^{137}Cs and 10 μCi ^{60}Co.

Acknowledgments

Funding: The work at Los Alamos National Laboratory (LANL) was supported by the LANL Directed Research and Development (LDRD) Funds (20180026DR) and performed in part at the Center for Integrated Nanotechnologies (CINT), a U.S. Department of Energy, Office of Science user facility at LANL. LANL is operated

by Triad National Security, LLC, for the National Nuclear Security Administration of the U.S. Department of Energy (Contract No. 89233218NCA000001).

Appendix A. Supplementary data

Supplementary data to this article can be found online at https://doi.org/10.1016/j.mattod.2020.02.022.

References

[1] M. Hoheisel, Nucl. Instrum. Meth. A 563 (2006) 215.
[2] Y. Eisen et al., Nucl. Instrum. Meth. A 428 (1999) 158.
[3] M.L. McConnell et al., J. Phys. Conf. Ser. 763 (2016) 012008.
[4] J. Knödlseder, C. R. Phys. 17 (2016) 663.
[5] V. B. Mykhaylyk, et al., Mater. Horiz. (2019).
[6] T. Hatsui, H. Graafsma, IUCrJ 2 (2015) 371.
[7] R. Carchon et al., Nucl. Instrum. Meth. A 579 (2007) 380.
[8] P.J. Sellin, Nucl. Instrum. Meth. A 513 (2003) 332.
[9] T.E. Schlesinger, R.B. James, Semiconductors for Room Temperature Nuclear Detector Applications.V43, 1st ed. Academic Press: San Diego, Calif, 1995.
[10] C.M. Davisson, R.D. Evans, Rev. Mod. Phys. 24 (1952) 79.
[11] M. Prokesch, et al., 124 (2018) 044503.
[12] R. Zhuang et al., Nat. Photonics (2019).
[13] Y. Zhang et al., ACS Nano 13 (2019) 2520.
[14] V. Morad et al., J. Am. Chem. Soc. 141 (2019) 9764.
[15] Y. He et al., ACS Photonics 5 (2018) 4132.
[16] Q. Chen et al., Nature 561 (2018) 88.
[17] W. Wei et al., Nat. Photonics 11 (2017) 315.
[18] S. Shrestha et al., Nat. Photonics 11 (2017) 436.
[19] W. Pan et al., Nat. Photonics 11 (2017) 726.
[20] Y.C. Kim et al., Nature 550 (2017) 87.
[21] H. Wei et al., Nat. Photonics 10 (2016) 333.
[22] S. Yakunin et al., Nat. Photonics 9 (2015) 444.
[23] Y. He et al., Nat. Commun. 9 (2018) 1609.
[24] H. Wei et al., Nat. Mater. 16 (2017) 826.
[25] O. Nazarenko et al., NPG Asia Mater. 9 (2017) e373.
[26] S. Yakunin et al., Nat. Photonics 10 (2016) 585.
[27] D. Shi et al., Science 347 (2015) 519.
[28] M.I. Saidaminov et al., Nat. Commun. 6 (2015) 7586.
[29] I. P. Zvyagin, 58 (1973) 443.
[30] N. Karl, Synth. Met. 133–134 (2003) 649.
[31] P.N. Murgatroyd, J. Phys. D Appl. Phys. 3 (1970) 151.
[32] Z. B. Wang, et al., 95 (2009) 043302.
[33] C. Eames et al., Nat. Commun. 6 (2015) 7497.
[34] W. Tress et al., Energy Environ. Sci. 8 (2015) 995.
[35] S. Meloni et al., Nat. Commun. 7 (2016) 10334.
[36] M.H. Futscher et al., Mater. Horiz. 6 (2019) 1497.
[37] O. Almora et al., J. Phys. Chem. Lett. 6 (2015) 1645.
[38] J.M. Ball, A. Petrozza, Nat. Energy 1 (2016) 16149.
[39] K.-H. Wang et al., Sci. Rep. 7 (2017) 13643.
[40] K. Galkowski et al., Energy Environ. Sci. 9 (2016) 962.
[41] A.M. Soufiani et al., Appl. Phys. Lett. 107 (2015) 231902.